

A novel $\text{Sm}_{0.5}\text{Sr}_{0.5}\text{Co}_{1-x}\text{Fe}_x\text{O}_{3-\delta}$ /acetylene black composite as bifunctional electrocatalyst for oxygen reduction/evolution reactions

Liquan Fan*, Tao Cong, Xinyu Su, Yuwei Wang, Xingmei Liu, Weichao Zhang, Yufeng Li, Deqing Zhang

College of Materials Science and Engineering, Heilongjiang Provincial Key Laboratory of Polymeric Composite Materials, Qiqihar University, No.42, Wenhua Street, Qiqihar 161006, PR China

*E-mail: Liquan_Fan@163.com

Received: 3 March 2021 / Accepted: 20 April 2021 / Published: 31 May 2021

The development of high efficient perovskite/carbon composite catalysts is an important means to improve the performance of clean energy devices such as metal-air batteries. For this reason, we report a bi-functional $\text{Sm}_{0.5}\text{Sr}_{0.5}\text{Co}_{1-x}\text{Fe}_x\text{O}_{3-\delta}$ /acetylene black composite electrocatalyst, consisting of the $\text{Sm}_{0.5}\text{Sr}_{0.5}\text{Co}_{1-x}\text{Fe}_x\text{O}_{3-\delta}$ (SSCF) nanofibers and acetylene black (AB). Owing to the electronic coupling effect of Fe and Co and the spillover effect of AB on $\text{Sm}_{0.5}\text{Sr}_{0.5}\text{Co}_{1-x}\text{Fe}_x\text{O}_{3-\delta}$, SSCF/AB exhibits outstanding OER and ORR performance. In 0.1M KOH solution, the OER Tafel slope of the SSCF/AB catalyst with the optimal mass ratio is 66.7 mV dec^{-1} , the ORR Tafel slope is $129.6 \text{ mV dec}^{-1}$. And after 1000 CV cycles, the stability performance of the catalyst remains good.

Keywords: OER/ORR; Air electrode; $\text{Sm}_{0.5}\text{Sr}_{0.5}\text{Co}_{1-x}\text{Fe}_x\text{O}_{3-\delta}$; Nanofibers

1. INTRODUCTION

How to develop new energy and renewable energy technologies is a common worldwide topic. Metal-air batteries are regarded as one of the most important means to realize renewable energy. Oxygen reduction reaction (ORR) and oxygen evolution reaction (OER) are extremely important reactions among these advanced electrochemical energy conversion technologies[1,2]. So far, the excellent ORR or OER catalysts are precious metal catalysts, such as Pt, Au, Ir, Ru, and Pd, and their alloys or oxides. However, they exist a lot of problems such as high price, scarcity, instability. Therefore, it is necessary to develop highly efficient, stable, non-precious metal bifunctional electrocatalysts[3].

Perovskite oxides show a broad application prospect for solid oxide fuel cells and metal-air cells because of their unique crystal structure after doping, which will form crystal defects and produce excellent catalytic properties. Recently, some nanostructured perovskite oxides have shown good

performance for solid oxide fuel cells, such as $\text{Sm}_{0.2}\text{Ce}_{0.9}\text{O}_{1.9}$ [4], $\text{Sm}_{0.5}\text{Sr}_{0.5}\text{CoO}_{3-\delta}$ [5], $\text{BaZr}_{0.4}\text{Ce}_{0.4}\text{Y}_{0.2}\text{O}_{3-\delta}$ [6], $\text{SrSc}_{0.175}\text{Ta}_{0.025}\text{Co}_{0.8}\text{O}_{3-\delta}$ [7], $\text{Ba}_{0.4}\text{K}_{0.1}\text{Sr}_{0.5}\text{Co}_{0.8}\text{Fe}_{0.2}\text{O}_{3-\delta}$ [8], $\text{Bi}_{0.5}\text{Sr}_{0.5}\text{Fe}_{0.85}\text{Ti}_{0.15}\text{O}_{3-\delta}$ [9]. In the field of metal-air batteries, perovskites also exhibit outstanding electrochemical performance, $\text{Sm}_{0.5}\text{Sr}_{0.5}\text{CoO}_{3-\delta}$ [10], $\text{Ba}_{0.5}\text{Sr}_{0.5}\text{Co}_{0.8}\text{Fe}_{0.2}\text{O}_{3-\delta}$ [11], $\text{La}_{1.5}\text{Sr}_{0.5}\text{NiMn}_{0.5}\text{Ru}_{0.5}\text{O}_6$ [12], $\text{PrBa}_{0.5}\text{Sr}_{0.5}\text{Co}_{1.5}\text{Fe}_{0.5}\text{O}_{5+\delta}$ [13], and $\text{Sr}_{0.95}\text{Co}_{0.8}\text{Fe}_{0.2}\text{O}_{3-\delta}$ [14] are typical representatives. So far, $\text{Ba}_{0.5}\text{Sr}_{0.5}\text{Co}_{0.8}\text{Fe}_{0.2}\text{O}_{3-\delta}$ is the best perovskite material with OER performance. The traditional preparation methods of perovskite oxides are usually sol-gel and solid-state reaction methods. These fabrication methods not only consume energy and time, but also pollutes the environment, and the prepared perovskites have a small specific surface area and few active sites, and general electrocatalytic performance. The perovskite oxide $\text{Sm}_{0.5}\text{Sr}_{0.5}\text{CoO}_{3-\delta}$ shows good performance in solid oxide fuel cells[15] and metal-air batteries[10]. When the molar ratio of Sm, Sr, and Co is 0.5:0.5:1, the conductivity reaches the highest value[5]. Herein, we applied the electrospinning method to prepare $\text{Sm}_{0.5}\text{Sr}_{0.5}\text{Co}_{1-x}\text{Fe}_x\text{O}_{3-\delta}$ (SSCF) perovskite nanofibers with a larger specific surface area and more effective active sites. Introducing acetylene black by ultrasonic mixing to SSCF, the ORR and OER performance of SSCF/acetylene black are investigated.

2. EXPERIMENTAL SECTION

2.1. Preparation of catalysts

$\text{Sm}_{0.5}\text{Sr}_{0.5}\text{Co}_{1-x}\text{Fe}_x\text{O}_{3-\delta}$ (SSCF, $x = 0.2, 0.4, 0.6, 0.8$) nanofibers were prepared by electrostatic spinning. The required chemicals are samarium nitrate ($\text{Sm}(\text{NO}_3)_3 \cdot 6\text{H}_2\text{O}$, content $\geq 99.9\%$), strontium nitrate ($\text{Sr}(\text{NO}_3)_2$, content $\geq 99.9\%$), cobalt nitrate ($\text{Co}(\text{NO}_3)_2 \cdot 6\text{H}_2\text{O}$, content $\geq 99.9\%$), iron nitrate ($\text{Fe}(\text{NO}_3)_3 \cdot 9\text{H}_2\text{O}$, content $\geq 99.9\%$), N,N-dimethylformamide (DMF, content $\geq 99.9\%$), polyvinylpyrrolidone (PVP, $M_w \approx 1300000$). DMF was used as a solvent, PVP as a binder, and metal nitrate of 10 wt% as a solute to form the electrospinning solution. The as-electrospun products were calcined at $800\text{ }^\circ\text{C}$ with a rate of $3\text{ }^\circ\text{C min}^{-1}$ in air and kept at $800\text{ }^\circ\text{C}$ for 2 h to develop $\text{Sm}_{0.5}\text{Sr}_{0.5}\text{Co}_{0.2}\text{Fe}_{0.8}\text{O}_{3-\delta}$, $\text{Sm}_{0.5}\text{Sr}_{0.5}\text{Co}_{0.4}\text{Fe}_{0.6}\text{O}_{3-\delta}$, $\text{Sm}_{0.5}\text{Sr}_{0.5}\text{Co}_{0.6}\text{Fe}_{0.4}\text{O}_{3-\delta}$, and $\text{Sm}_{0.5}\text{Sr}_{0.5}\text{Co}_{0.8}\text{Fe}_{0.2}\text{O}_{3-\delta}$ nanofibers (denoted as SSCF28, SSCF46, SSCF64, and SSCF82, respectively). SSCF28 and acetylene black (AB) were uniformly mixed by sonication to prepare SSCF28/AB composite catalysts with different mass ratios (SSCF28: AB=1:3, 1:2, 1:1, 2:1, 3:1).

2.2 Electrochemical characterization

3 mg of catalyst powder was dispersed in 1 mL of Nafion aqueous solution (0.5 wt%), and subsequently sonicated for 30 min to generate a homogeneous 3 mg mL^{-1} catalyst suspension. $10\text{ }\mu\text{L}$ of the catalyst suspension was drop-casted onto a 4mm diameter glassy carbon electrode (GCE), and then kept at room temperature for 1 h, forming a membrane. The surface area of the as-modified GCE was 0.1256 cm^2 .

Electrochemical tests were performed on a rotating ring disk electrode device (RRDE, ALS Co., Ltd.). GCE is used as the working electrode, Ag/AgCl as the reference electrode, and platinum wire as the counter electrode. For ORR/OER test, 0.1 M KOH solution was used as the electrolyte, the electrode speed was 1600 rpm, and the scanning speed was 5 mV s^{-1} . The electron transfer number (n) can be calculated out during the ORR process and the relative formula can be found in reference[16,17].

3. RESULTS AND DISCUSSION

To evaluate the optimal ratio of Co: Fe in $\text{Sm}_{0.5}\text{Sr}_{0.5}\text{Co}_{1-x}\text{Fe}_x\text{O}_{3-\delta}$ catalysts, four kinds of $\text{Sm}_{0.5}\text{Sr}_{0.5}\text{Co}_{1-x}\text{Fe}_x\text{O}_{3-\delta}$ perovskite nanofibers with different Co: Fe molar ratio were prepared by electrospinning and subsequently calcination. The SEM test results are shown in Fig. 1. As shown in Fig. 2(a), the XRD patterns for four kinds of the SSCF nanofibers have similar peaks position that can be well indexed to $\text{Sm}_{0.5}\text{Sr}_{0.5}\text{CoO}_{3-\delta}$ (PDF#53-0112), indicating their good crystallization. Fig. 2(b) shows a comparison of X-ray peaks between diffraction angle 2θ values of 30° and 37° of spectra taken from Fig. 2(a). With the increase of iron content, the characteristic peak gradually shifts to a small angle direction. This is because Co^{3+} is replaced by larger Fe^{3+} , which causes the lattice expansion of the perovskite unit cell[18].

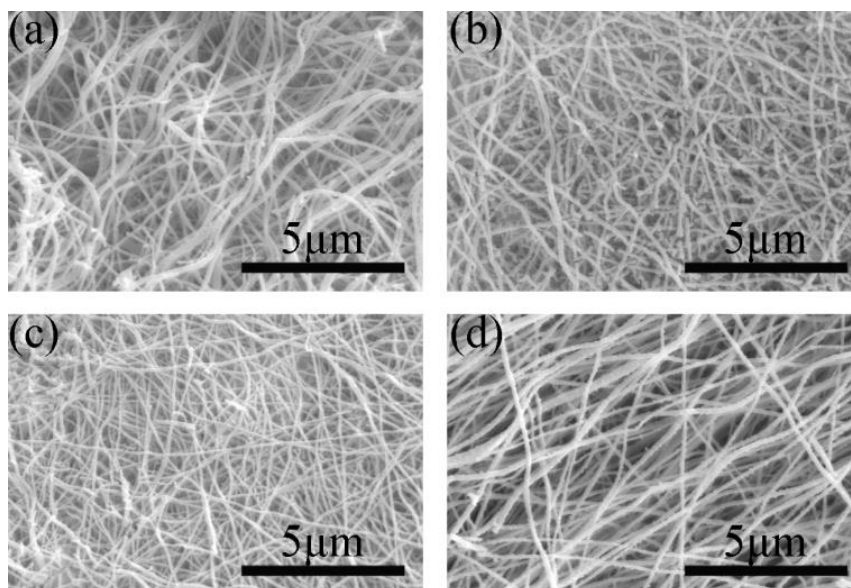


Figure 1. SEM images of (a) SSCF28, (b) SSCF46, (c) SSCF64, and (d) SSCF82

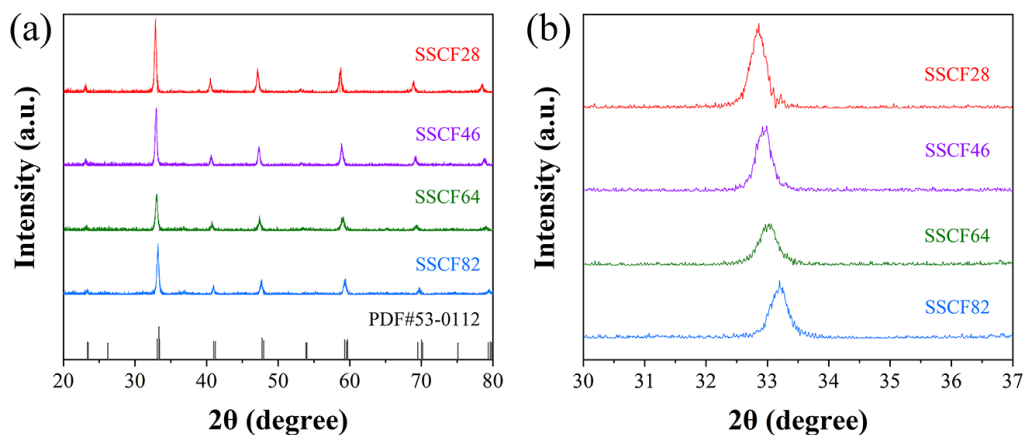


Figure 2. XRD patterns of SSCF after calcination at 800°C for 2h.

Fig. 3 shows the high-resolution XPS spectra of Co 2p, Fe 2p, and O 1s of the SSCF catalysts. As shown in Fig. 3(a), the high-resolution spectra of Co 2p can be divided into six peaks. The peaks at 780.06 eV and 795.1 eV can be distributed to Co^{3+} . The peaks at 781.2 eV and 796.6 eV represent Co^{2+} , and the positions at 786.6-790.5 eV and 802.7-805.6 eV belong to satellite peaks[19]. According to the literature[14], Co^{3+} is more favorable to catalytic reaction, and more Co^{3+} can improve the OER performance of the catalyst. The catalytic activity of the catalyst can be analyzed by the ratio of $\text{Co}^{3+}/\text{Co}^{2+}$. The $\text{Co}^{3+}/\text{Co}^{2+}$ values of SSCF are summarized in Table 1. As seen from Fig. 3(b), the peaks at 710.7 eV and 724.5 eV can be attributed to Fe^{3+} [20]. The high-resolution spectra of O 1s can be divided into three peaks.

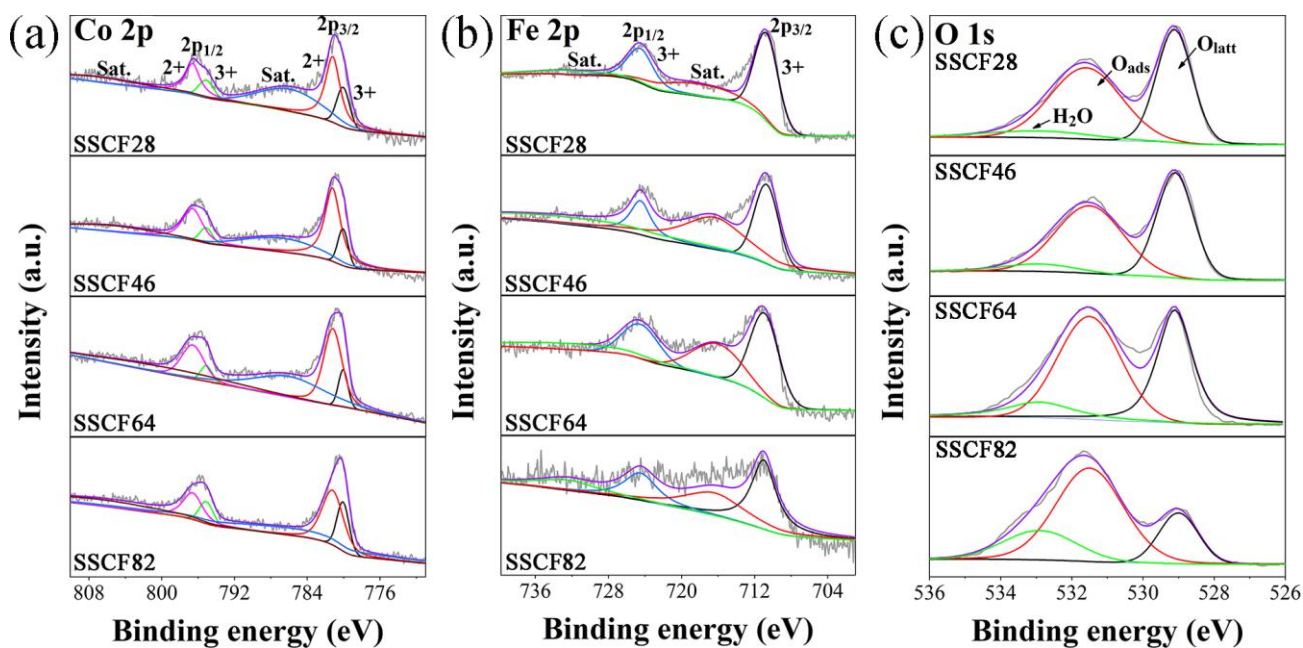


Figure 3. High-resolution XPS spectra of SSCF catalysts. (a) Co 2p, (b) Fe 2p, (c) O 1s.

Table 1. The $\text{Co}^{3+}/\text{Co}^{2+}$ ratios of SSCF.

Samples	Ratio ($\text{Co}^{3+}/\text{Co}^{2+}$)
SSCF28	0.856
SSCF46	0.641
SSCF64	0.508
SSCF82	0.609

As shown in Fig. 3(c), the peaks at 529.1, 531.6, 532.9 eV correspond to the lattice $\text{O}^{2-}(\text{O}_{\text{latt}})$, $\text{O}_2^{2-}/\text{O}^-(\text{O}_{\text{ads}})$, and the adsorbed water (H_2O), respectively[21]. $\text{O}_2^{2-}/\text{O}^-$ is an important electron transfer step in the OER process, and the ratios of $\text{O}_{\text{ads}}/\text{O}_{\text{latt}}$ (Table 2) can be used to reliably analyze the catalytic activity of the catalyst[19]. The peak at 531.6 eV represents -OH. The hydroxyl group plays a key role in the OER process, accelerating the formation of O-O bonds and increasing oxygen production rate[21]. The adsorbed water depends to a large extent on the atmospheric pressure rather than the catalyst itself, so it was not discussed here[22]. By contrast, SSCF28 has the best catalytic activity. XPS peaks deconvolution results of SSCF28 is shown in Table 3.

Table 2. The $\text{O}_{\text{ads}}/\text{O}_{\text{latt}}$ ratios of SSCF.

Samples	Ratio ($\text{O}_{\text{ads}}/\text{O}_{\text{latt}}$)
SSCF28	1.978
SSCF46	1.833
SSCF64	1.776
SSCF82	1.716

Table 3. XPS peaks deconvolution results of SSCF28.

Species	Banding energy (eV)		
Co 2p	2p _{3/2}	Co^{3+}	780.06
		Co^{2+}	781.2
		Sat.	786.6~790.5
	2p _{1/2}	Co^{3+}	795.1
		Co^{2+}	796.6
		Sat.	802.7-805.6
Fe 2p	2p _{3/2}	Fe^{3+}	710.7
		Sat.	716.4~717.8
	2p _{1/2}	Fe^{3+}	724.5
		Sat.	730.9~732.5
O 1s	O_{ads}	531.6	
	O_{latt}	529.1	
	H_2O	532.9	

The continuous and uniform SSCF28 nanofibers prepared by electrospinning are presented in Fig. 4 (a). It appeared a three-dimensional network structure with a large specific surface area and plenty of oxygen transport paths. As shown in Fig. 4 (b) and (c), the TEM and SEM measurements results indicate that the AB particles are well intersected into the SSCF28 nanofibers scaffolds through ultrasonic mixing to form SSCF28/AB composite catalyst. Fig. 4 (c1)-(c6) are EDS images of SSCF28/AB (SSCF28: AB mass ratio of 2:1, both here and below), which clearly show the uniform distribution of Sm, Sr, Co, Fe, O and C elements. It further proves that AB has been well dispersed in the three-dimensional network framework of SSCF28 nanofibers.

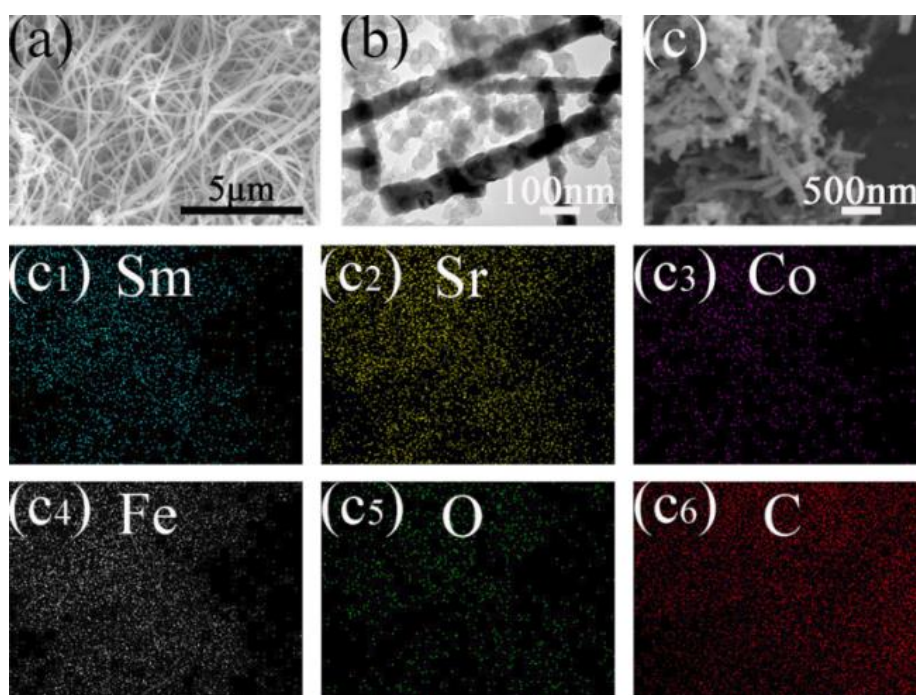


Figure 4. (a) SEM image of SSCF28. (b) TEM image of SSCF28/AB. (c) SEM image of SSCF28/AB. (c1)-(c6) EDS element mappings of Fig. 4(c).

To evaluate the effect of Co: Fe molar ratio on the electrochemical performance of $\text{Sm}_{0.5}\text{Sr}_{0.5}\text{Co}_{1-x}\text{Fe}_x\text{O}_{3-\delta}$, their OER and ORR activities were respectively investigated. As shown in Fig. 5(a), the OER performance of SSCF rapidly increases with the Fe content in SSCF. Amongst them, the potential of SSCF28 reached the highest value, 1.792V at 10 mA cm^{-2} . The OER Tafel slopes of SSCF28, SSCF46, SSCF64, and SSCF82 are respectively 86.7, 97.3, 109.0, and 130.9 mV dec^{-1} (see Fig. 5(b)). Fig. 5(c) shows the electrochemical impedance spectra (EIS) of SSCF. With the increase of Fe content in SSCF, the EIS values of SSCF decreases significantly, and SSCF28 shows the smallest value. Fig. 5(d) is the polarization curve of SSCF during ORR process. The ORR activity of SSCF82 is weaker than the other three samples. As shown in Fig. 5(e), the ORR Tafel slopes of SSCF28, SSCF46, SSCF64, and SSCF82 are respectively 133.7, 128.7, 129.2, and 138.6 mV dec^{-1} . As shown in Fig. 5(f), the electron-transfer number of SSCF28 is closest to 4. Combined ORR with OER analysis results, it can be seen that SSCF28 has the best electrochemical performance, in agreement with XPS analysis. Fe and Co have a strong

electronic coupling effect in the solid[23,24]. The clear implication of these results is that the electrocatalytic performance of $\text{Sm}_{0.5}\text{Sr}_{0.5}\text{CoO}_{3-\delta}$ can be enhanced significantly by the moderate doping of Fe element.

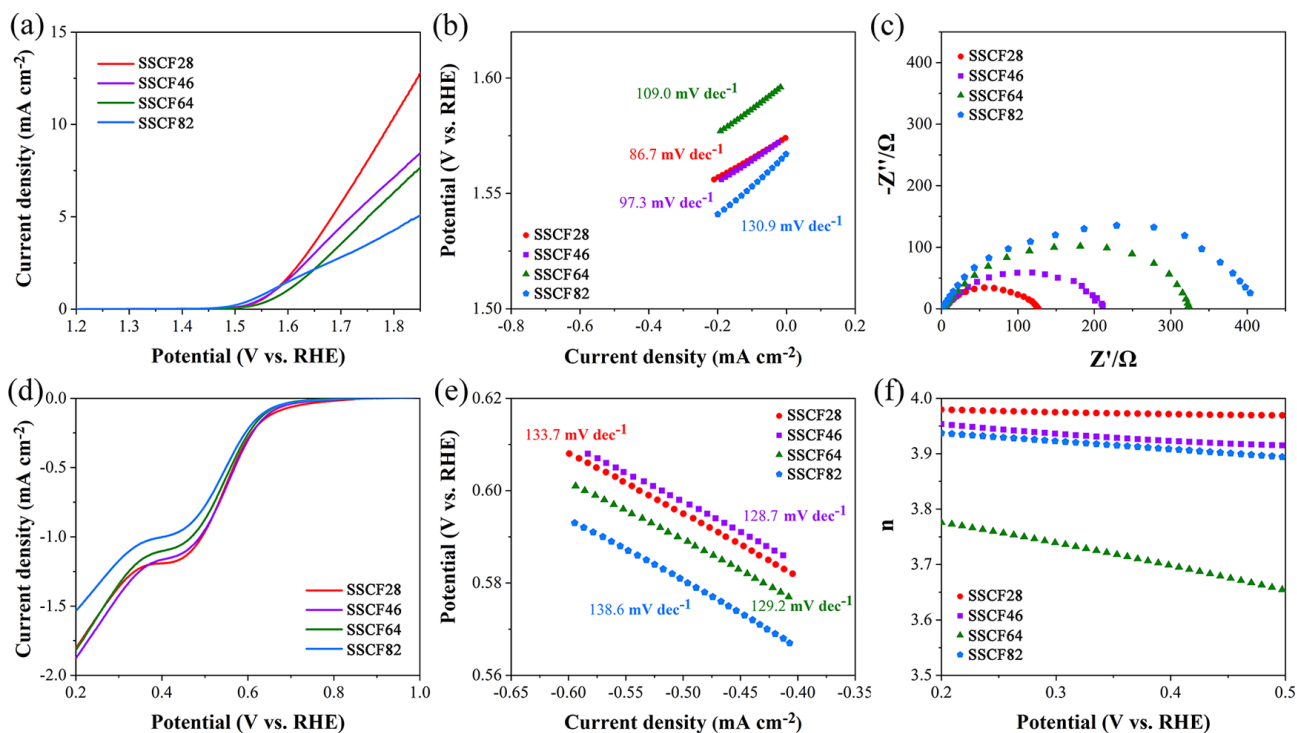


Figure 5. OER and ORR activities of SSCF. (a) Polarization curve of OER activity. (b) Tafel plots obtained from the polarization curves in OER process. (c) Electrochemical impedance spectra at 1.664 V (vs. RHE). (d) Polarization curve of ORR activity. (e) Tafel plots obtained from the polarization curves in ORR process. (f) Electron-transfer number of SSCF.

To prove whether the addition of AB can enhance the electrocatalytic performance of SSCF, the OER performance of SSCF28/AB with different mass ratios was tested. As shown in Fig. 6(a), compared with phase pure SSCF28, the addition of AB greatly enhances the catalytic performance of SSCF28, and the $E_{10\text{mA cm}^{-2}}$ of SSCF/AB (2: 1) reaches the maximum value of 1.665 V. Fig. 6(b) shows the Tafel plots of SSCF28/AB with the various mass ratios of SSCF28 to AB. The Tafel slope of SSCF28/AB (2: 1) shows the lowest value of 66.7 mV dec⁻¹, which is greater than the comparable reported values. Zhang et al[25] reported that $E_{10\text{mA cm}^{-2}}$ was 1.83 V and the Tafel slope was 186 mV dec⁻¹ for the SSC/conductive carbon composite catalyst. The Tafel slope of SSC/three-dimensional nitrogen-doped graphene composite catalyst prepared by Bu et al. is 115mV dec⁻¹[10]. Fig. 6(c) and (d) present EIS of SSCF28/AB and AB, respectively. It can be seen that the resistance of SSCF28/AB (2: 1) is only 27 Ω, smaller than that of SSCF28, indicating that the addition of AB successfully improves the electronic conductivity of SSCF28[25]. As expected, measurements have shown that the OER activity of SSCF/AB (2: 1) is much better than the other three composites, SSCF28 and AB. The adding of AB particles filled the gaps of SSCF28 nanofibers, and the carbon phase provided a conductive network and connected the perovskite

phase. The formation of the close interface between the perovskite and carbon phase is the key to realize the effective electron transfer in the composite electrode, which is beneficial to the electrocatalytic reaction[26]. In addition to the conductive enhancement of AB on SSCF28, it also benefits spillover effect on perovskite and carbon[26]. During the OER process, the perovskite SSCF28 plays a leading role. Excessive oxygen spills onto the surface of AB, releasing more active sites on the surface of SSCF28 perovskite. As summarized in Table 4, compared with to other similar kinds of perovskite/C composite catalysts, SSCF28/AB (2:1) still has excellent OER activity.

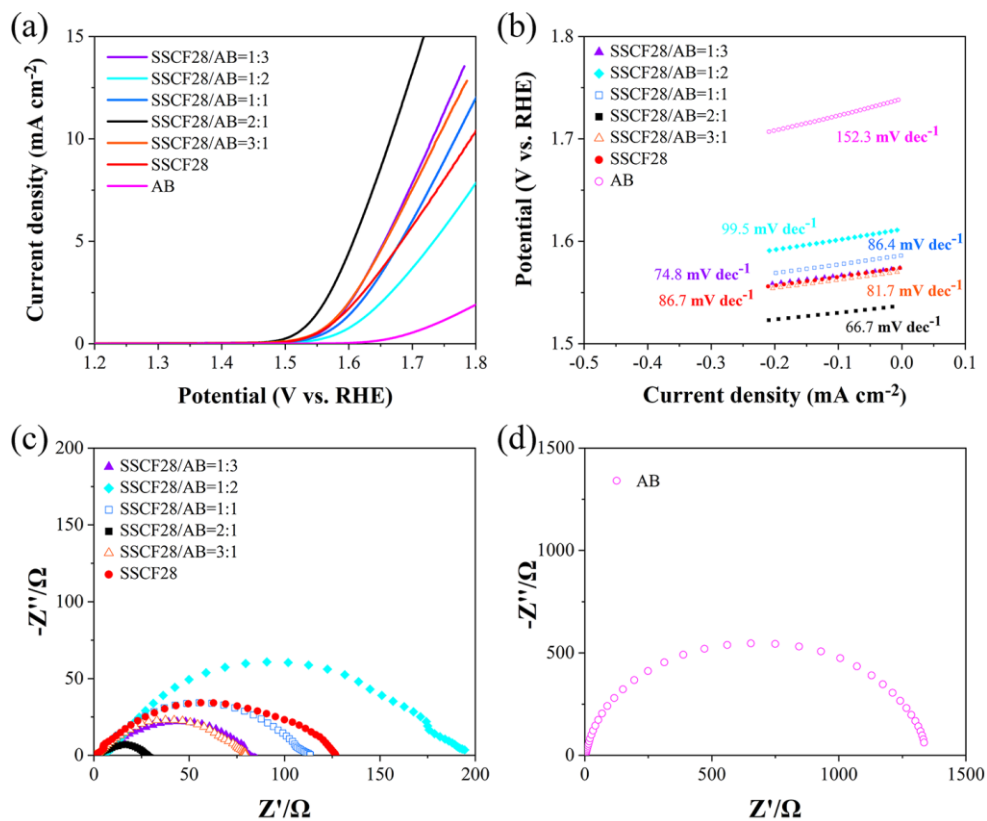


Figure 6. OER activity of SSCF28/AB. (a) Polarization curve. (b) Tafel plots obtained from the polarization curves in OER process. (c) and (d) are EIS of SSCF28/AB and AB at 1.664 V (vs. RHE), respectively.

Table 4. Comparison of OER activity of perovskite/carbon composite catalysts.

Catalyst	E_{OER} at 10 mA cm ⁻² (V)	Ref.
SSCF28/AB (2:1)	1.665 vs. RHE	This work
SSC/3DNG	1.63 vs. RHE	[10]
Nanostructured LaNiO ₃ nanorod/NC	1.66 vs. RHE	[27]
PrBaMn ₂ O _{5+δ} /C	1.73 vs. RHE	[28]
La _{0.5} Sr _{0.5} CoO _{2.91} nanowire/AC (XC-72)	1.83 vs. RHE	[29]
La _{0.5} Sr _{0.5} Co _{0.8} Fe _{0.2} O ₃ nanorod/NRGO	1.73 vs. RHE	[30]
LaNiO ₃ nanoparticle/NCNT	1.74 vs. RHE	[31]
LaTi _{0.65} Fe _{0.35} O _{3-δ} nanorod/NCNR	1.77 vs. RHE	[32]

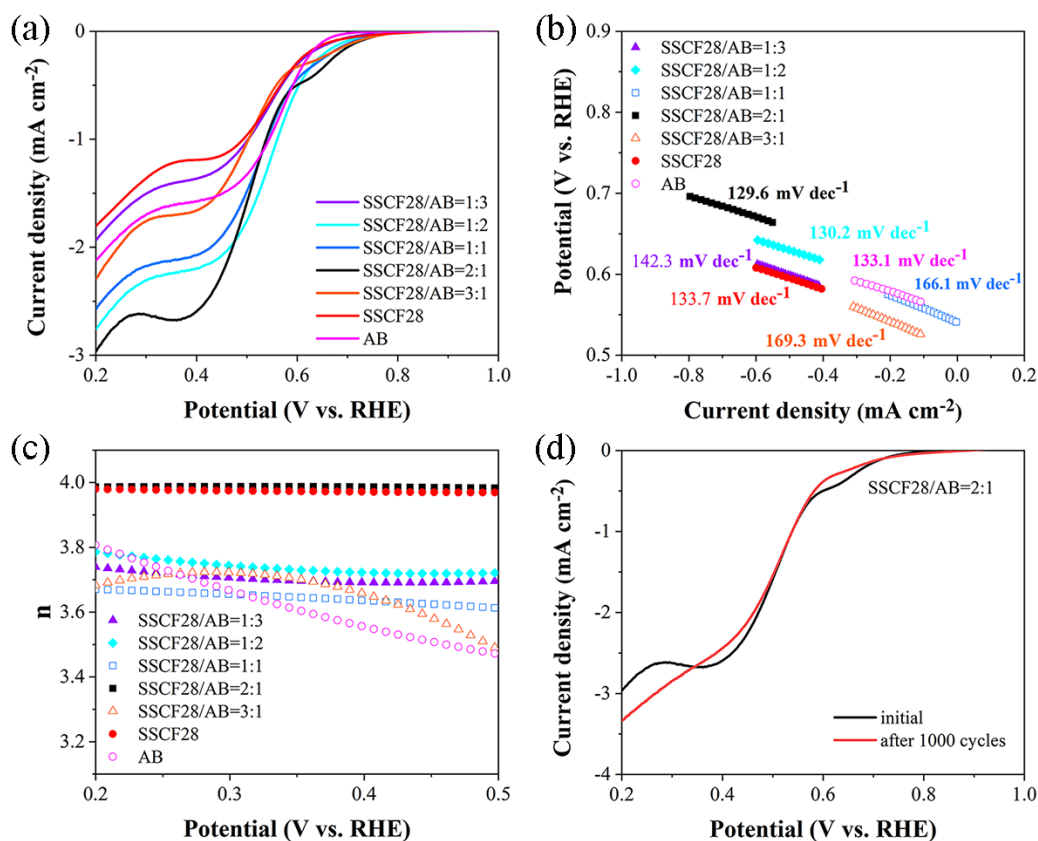


Figure 7. ORR activity of SSCF28/AB. (a) Polarization curve. (b) Tafel plots obtained from the polarization curves in ORR process. (c) The electron-transfer numbers. (d) Accelerated durability test of SSCF28/AB.

Fig. 7(a) illustrates ORR LSV curves for the SSCF catalysts with different SSCF28: AB mass ratios. By contrast, SSCF28/AB shows the biggest current density of 2.97 mA cm⁻² at 0.2 V and the highest half-wave potential of 0.51 V. Fig. 7(b) shows the Tafel plots of SSCF28/AB obtained from the polarization curves in ORR process. The Tafel slope of SSCF28/AB (2:1) shows the lowest value of 129.6 mV dec⁻¹, compared to the other samples. This indicates SSCF28/AB (2:1) has the optimal ORR activity. As can be seen from Fig. 7(c), the electron-transfer number of SSCF/AB (2:1) in the 0.2-0.5V potential range is closest to 4. To determine whether SSCF/AB composite electrocatalyst is practical or not, the cycle stability of SSCF28/AB with optimal electrocatalytic performance was verified by an accelerated durability test (ADT). After 1000 CV cycles in the potential range of 0.2 to -0.8 V obtain a new ORR LSV curve[25]. After 1000 CV cycles, the current density of the catalyst was 3.35 mA cm⁻² at 0.2 V and the half-wave potential was 0.49 V, shown in Fig. 7(d). The SSCF28/AB electrocatalyst showed excellent stability. The spillover effect is not only reflected in OER but also ORR process. In the ORR reaction process dominated by AB, excess OH⁻ spills from the surface of AB to the surface of SSCF, which will release more active sites on the surface of AB[26].

4. CONCLUSIONS

A highly efficient bifunctional electrocatalyst was prepared by uniformly mixing SSCF28 nanofibers and AB by ultrasonic wave. The OER and ORR processes show a low Tafel slope, four electron-transfer numbers, and excellent stability. The excellent electrochemical properties are mainly due to the synergistic effect of perovskite oxide SSCF28 and AB. This novel bifunctional oxygen electrocatalyst SSCF28/AB with high efficiency, economy, and environmental protection has a potential application prospect in the field of metal-air batteries.

ACKNOWLEDGMENTS

The Natural Science Foundation of Heilongjiang Province, China (No. LH2019E092), and the Fundamental Research Funds in Heilongjiang Provincial Universities (No. 135309349).

References

1. Y. Liang, Y. Li, H. Wang, J. Zhou, J. Wang, T. Regier, H. Dai, *Nat. Mater.*, 10 (2011) 780–786.
2. J. Zhang, Z. Zhao, Z. Xia and L. Dai, *Nat. Nanotechnol.*, 10 (2015) 444–452.
3. Z. Chen, A. Yu, D. Higgins, H. Li, H. Wang, Z. Chen, *Nano Lett.*, 12 (2012) 1946–1952.
4. K. Gao, X. Liu, Z. Wang, Y. Xiong, *Int. J. Hydrogen Energy*, 42 (2017) 19170–19177.
5. R. Scurtu, S. Somacescu, J.M. Calderon-Moreno, D. Culita, I. Bulimestru, N. Popa, A. Gulea, P. Osiceanu, *J. Solid State Chem.*, 210 (2014) 53–59.
6. T. Kobayashi, K. Kuroda, S. Jeong, H. Kwon, C. Zhu, H. Habazaki, Y. Aoki, *J. Electrochem. Soc.*, 165 (2018) F342–F349.
7. X. Xu, J. Zhao, M. Li, L. Zhuang, J. Zhang, S. Aruliah, F. Liang, H. Wang, Z. Zhu, *Compos. Part B Eng.*, 178 (2019) 107491.
8. X. Xu, H. Wang, M. Fronzi, X. Wang, L. Bi, E. Traversa, *J. Mater. Chem. A*, 7 (2019) 20624–20632.
9. J. Gao, Q. Li, W. Xia, L. Sun, L.H. Huo, H. Zhao, *ACS Sustain. Chem. Eng.*, 7 (2019) 18647–18656.
10. Y. Bu, G. Nam, S. Kim, K. Choi, Q. Zhong, J.H. Lee, Y. Qin, J. Cho, G. Kim, *Small*, 14 (2018) 1802767.
11. G. Li, S. Hou, L. Gui, F. Feng, D. Zhang, B. He, L. Zhao, *Appl. Catal. B Environ.*, 257 (2019) 117919.
12. M. Retuerto, F. Calle-Vallejo, L. Pascual, G. Lumbeck, M.T. Fernandez-Diaz, M. Croft, J. Gopalakrishnan, M.A. Peña, J. Hadermann, M. Greenblatt, S. Rojas, *ACS Appl. Mater. Interfaces*, 11 (2019) 21454–21464.
13. H. Yu, F. Chu, X. Zhou, J. Ji, Y. Liu, Y. Bu, Y. Kong, Y. Tao, Y. Li, Y. Qin, *Chem. Commun.*, 55 (2019) 2445–2448.
14. Y. Da, L. Zeng, C. Wang, C. Gong, L. Cui, *Electrochim. Acta*, 300 (2019) 85–92.
15. L. Fan, Y. Xiong, L. Liu, Y. Wang, M.E. Brito, *Int. J. Electrochem. Sci.*, 8 (2013) 8603–8613.
16. H. Cheng, K. Xu, L. Xing, S. Liu, Y. Gong, L. Gu, L. Zhang, C. Wu, *J. Mater. Chem. A*, 4 (2016) 11775–11781.
17. H. Lee, O. Gwon, K. Choi, L. Zhang, J. Zhou, J. Park, J.W. Yoo, J.Q. Wang, J.H. Lee, G. Kim, *ACS Catal.*, 10 (2020) 4664–4670.
18. L. Li, J. Song, Q. Lu, X. Tan, *Ceram. Int.*, 40 (2014) 1189–1194.
19. Z. Wang, S. Tan, Y. Xiong, J. Wei, *Prog. Nat. Sci. Mater. Int.*, 28 (2018) 399–407.

20. W. Temesghen, P.M.A. Sherwood, *Anal. Bioanal. Chem.*, 373 (2002) 601–608.
21. Z. Wang, Y. You, J. Yuan, Y.X. Yin, Y.T. Li, S. Xin, D. Zhang, *ACS Appl. Mater. Interfaces*, 8 (2016) 6520–6528.
22. Q. Wang, Y. Xue, S. Sun, S. Li, H. Miao, Z. Liu, *Electrochim. Acta*, 254 (2017) 14–24.
23. M.S. Burke, M.G. Kast, L. Trotochaud, A.M. Smith, S.W. Boettcher, *J. Am. Chem. Soc.*, 137 (2015) 3638–3648.
24. R.D.L. Smith, C. Pasquini, S. Loos, P. Chernev, K. Klingan, P. Kubella, M.R. Mohammadi, D. Gonzalez-Flores, H. Dau, *Nat. Commun.*, 8 (2017) 2022.
25. Y. Zhang, Y. Guo, T. Liu, F. Feng, C. Wang, H. Hu, M. Wu, M. Ni, Z. Shao, *Front. Chem.*, 7 (2019) 524.
26. Y. Zhu, W. Zhou, Z. Shao, *Small*, 13 (2017) 1603793.
27. W. G. Hardin, D. A. Slanac, X. Wang, S. Dai, K. P. Johnston, K. J. Stevenson, *J. Phys. Chem. Lett.*, 4 (2013) 1254–1259.
28. D. Chen, J. Wang, Z. Zhang, Z. Shao, F. Ciucci, *Chem. Commun.*, 52 (2016) 10739–10742.
29. Y. Zhao, L. Xu, L. Mai, C. Han, Q. An, X. Xu, X. Liu, Q. Zhang, *Proc. Natl. Acad. Sci. U. S. A.*, 109 (2012) 19569–19574.
30. H. W. Park, D. U. Lee, P. Zamani, M. H. Seo, L. F. Nazar, Z. Chen, *Nano Energy*, 10 (2014) 192–200.
31. D. U. Lee, H. W. Park, M. G. Park, V. Ismayilov, Z. Chen, *ACS Appl. Mater. Interfaces*, 7 (2015) 902–910.
32. M. Prabu, P. Ramakrishnan, P. Ganesan, A. Manthiram, S. Shanmugam, *Nano Energy*, 15 (2015) 92–103.